Appendix C

SUPPLEMENTARY INFORMATION FOR "AN ON-PHASED ARRAY SYSTEM FOR NON-CLASSICAL LIGHT"

Our photonic integrated circuit (PIC) is one of the largest-scale PICs demonstrated in the literature with more than 1,000 functional components, as shown in Fig. C.1. Photos of the chip on top of a penny are shown in Fig. C.1a, and the packaged photonic-electronic system is shown in Fig. C.1b. Here, we provide a description of the PIC components and their characterization.

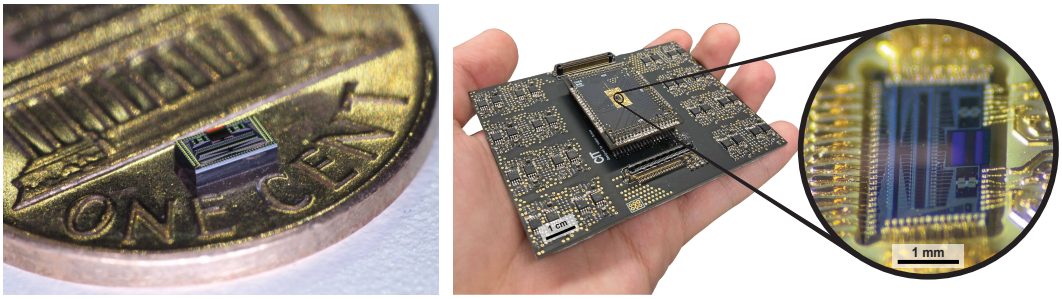

Figure C.1: Photo of the PIC on top of a penny (left). Photos of the packaged photonic-electronic system comprising the chip wirebonded to an interposer interfaced with an RF motherboard (right). The system can be packaged as a handheld device enabled by the integration and packaging of photonics and electronics.

C.1 On-chip squeezing analysis

Here we demonstrate how we extract the squeezing and antisqueezing levels for the experiments in Chapter 6 using the estimation procedure from Appendix B. We walk through the analysis of a chip data set using our estimation procedure and demonstrate how we extract the squeezing and antisqueezing levels for the experiments in Fig. 6.5 of Chapter 6. The complete analysis for the 32-channel source characterization data of Fig. 6.5c is shown in Figs. C.2-C.5 and the histograms for the remaining data of Fig. 6.5 are shown in Figs. C.6-C.9.

32-channel source characterization

For each pump power (P) of the 32-channel sweep in Fig. 6.5c, we measure noise power traces for the squeezed vacuum and vacuum states using an RF spectrum

analyzer with a 2 MHz RBW, 5 Hz VBW, and 1.25 kHz sampling rate. Each vacuum trace is taken immediately before or after a squeezed vacuum trace. For a pair of vacuum and squeezed vacuum traces, each trace is acquired over the same amount of time, typically over 5-10s. Due to random phase drifts, we acquire multiple pairs of vacuum and squeezed vacuum traces until an approximately uniform sampling of phases is achieved. To correct long-term drifts in the LO power, each pair is normalized by the mean of the vacuum trace. The normalized traces are concatenated to obtain squeezed vacuum and vacuum traces corresponding to an approximately uniform phase distribution (Fig. C.2). To perform the estimation procedure on the same number of points for all pump powers, 10^4 points are randomly sampled from each concatenated trace (Fig. C.3). The histograms are constructed for the sampled noise powers, and the PDFs are approximated by kernel density estimation (Fig. C.4). The squeezing and antisqueezed level estimates are obtained from the peaks in the derivative of the KDEs (Fig. C.5). The KDEs and their derivatives are compared with a theoretical model for a uniform phase distribution. The theoretical models are calculated from Eq. B.11 with $\sigma = 0.012$ dB, $\eta = 0.0157$, and $r = \mu\sqrt{P}$, where $\mu = 0.038\ [\mathrm{mW}]^{-1/2}$ (see Sec. C.2). The experimental estimates (blue), theoretical estimates (purple), and the noise floor (black) are indicated with dashed lines in Fig. C.3, Fig. C.4, and Fig. C.5. The experimental and theoretical estimates are in near agreement despite the phase noise in the measurements. We note that some discrepancies in the theoretical and experimental estimates are expected because the model fit was performed on the experimental estimates with only one free parameter across the entire data set rather than an individual fit to each histogram.

Beamforming

For each channel combination in Fig. 6.5b, we measure noise power traces for the squeezed vacuum and vacuum states using an RF spectrum analyzer with a 2 MHz RBW, 5 Hz VBW, and 1.25 kHz sampling rate. For each trace, 10^4 noise powers are sampled at random. The histograms and KDEs of the noise power samples for all channel combinations are shown in Fig. C.6.

Beamwidth

For each channel combination in Fig. 6.5e, we measure noise power traces for the squeezed vacuum and vacuum states using an RF spectrum analyzer with a 2 MHz RBW, 5 Hz VBW, and 625 Hz sampling rate. For each trace, 10^4 noise powers are sampled at random. The histograms and KDEs of the noise power samples for all

channel combinations are shown in Fig. C.7 for 8 channels combined and Fig. C.8 for 32 channels combined.

Field of view

For each channel combination in 6.5f, we measure noise power traces for the squeezed vacuum and vacuum states using an RF spectrum analyzer with a 2 MHz RBW, 5 Hz VBW, and 1 kHz sampling rate. For each trace, 10^4 noise powers are sampled at random. The histograms and KDEs of the noise power samples for all channel combinations are shown in Fig. C.9a for 8 channels combined and Fig. C.9b for 32 channels combined.

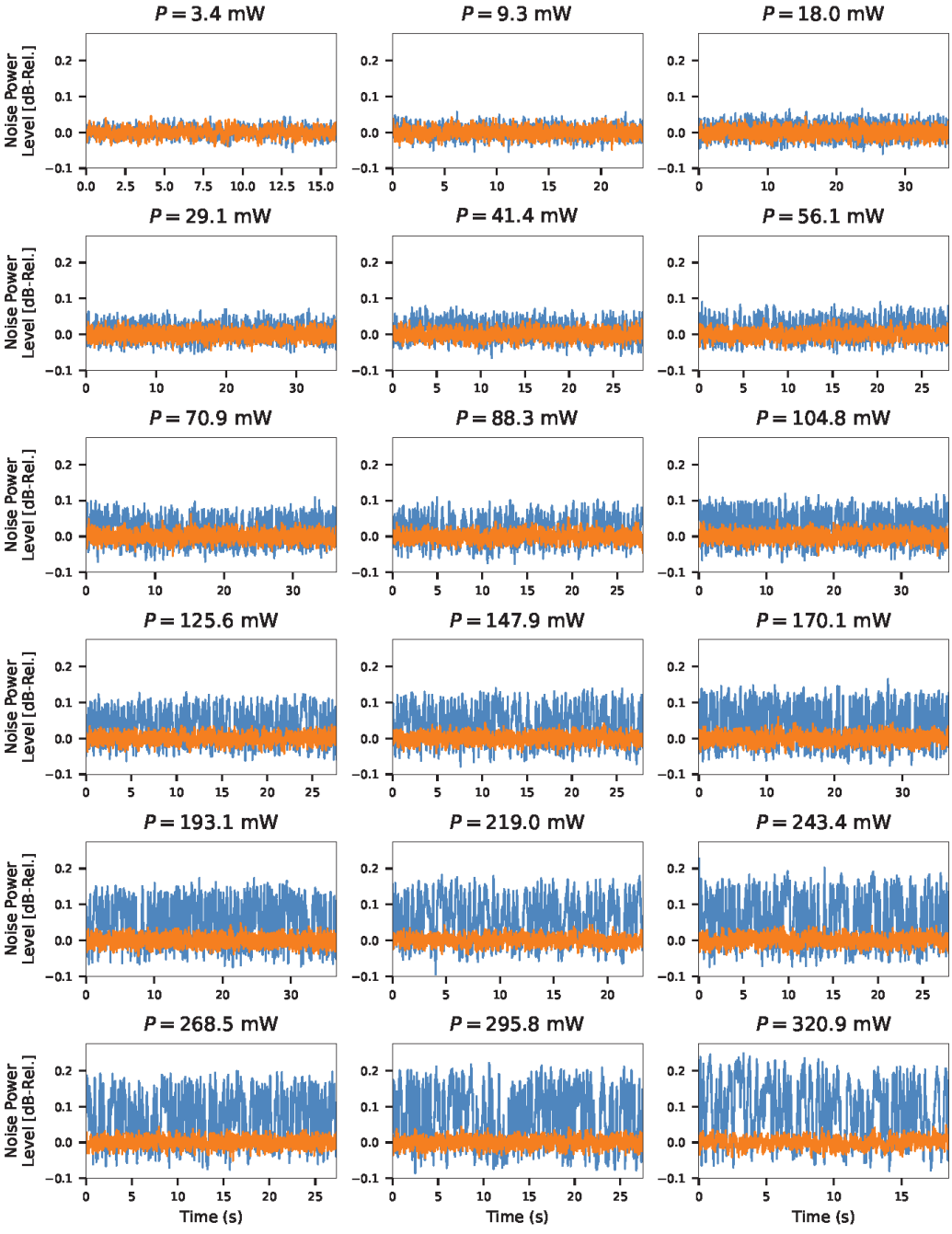

Figure C.2: Data analysis for the 32-channel source characterization in Fig. 6.5c: noise power traces for the squeezed vacuum (blue) and vacuum (orange) states.

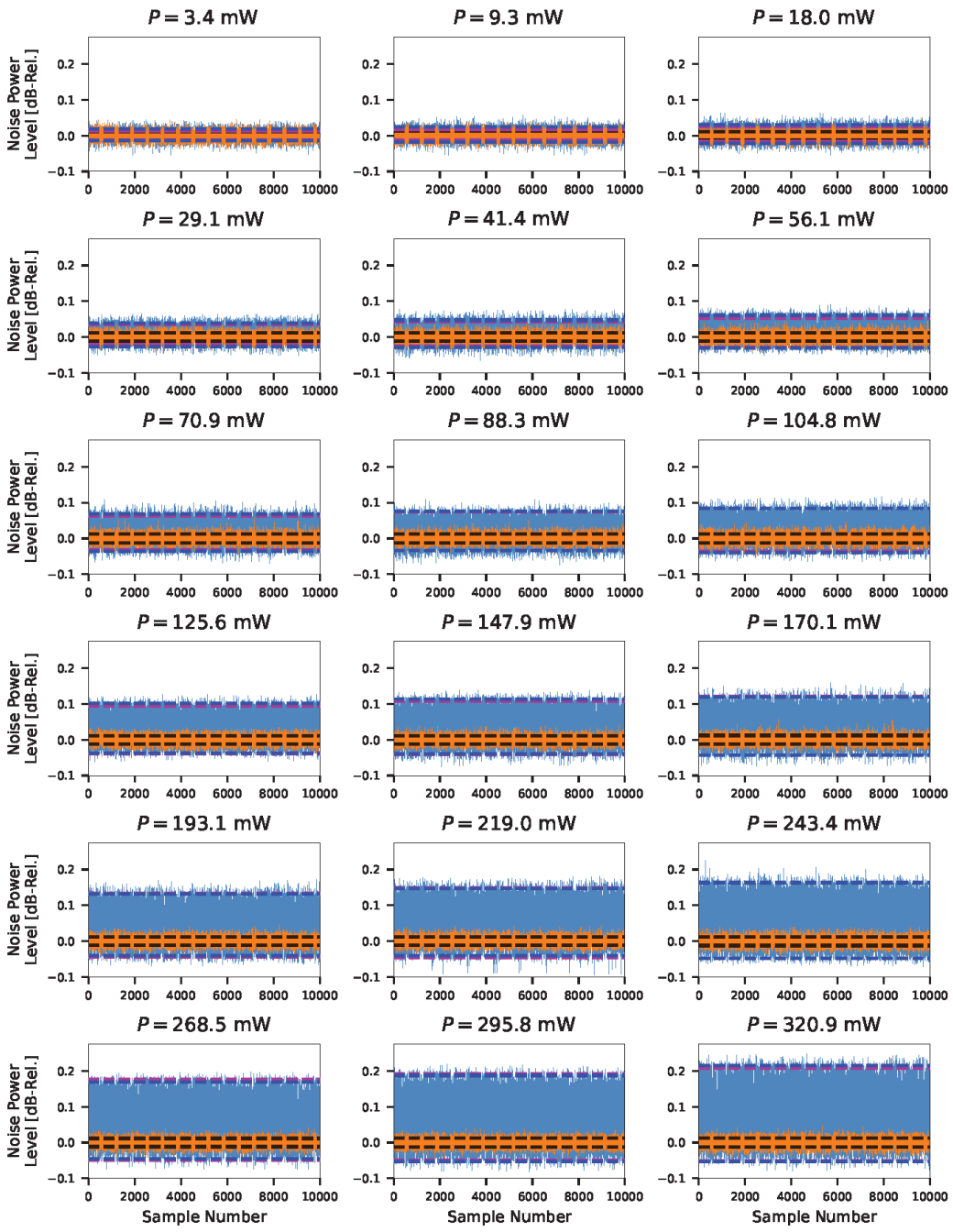

Figure C.3: Data analysis for the 32-channel source characterization in Fig. 6.5c: noise power samples for the squeezed vacuum (blue) and vacuum (orange) states are collected for various pump powers. The squeezing and antisqueezing level estimates are indicated with dashed blue lines, the theoretical model estimates are indicated with dashed purple lines, and the the shot noise floor is indicated with dashed black lines.

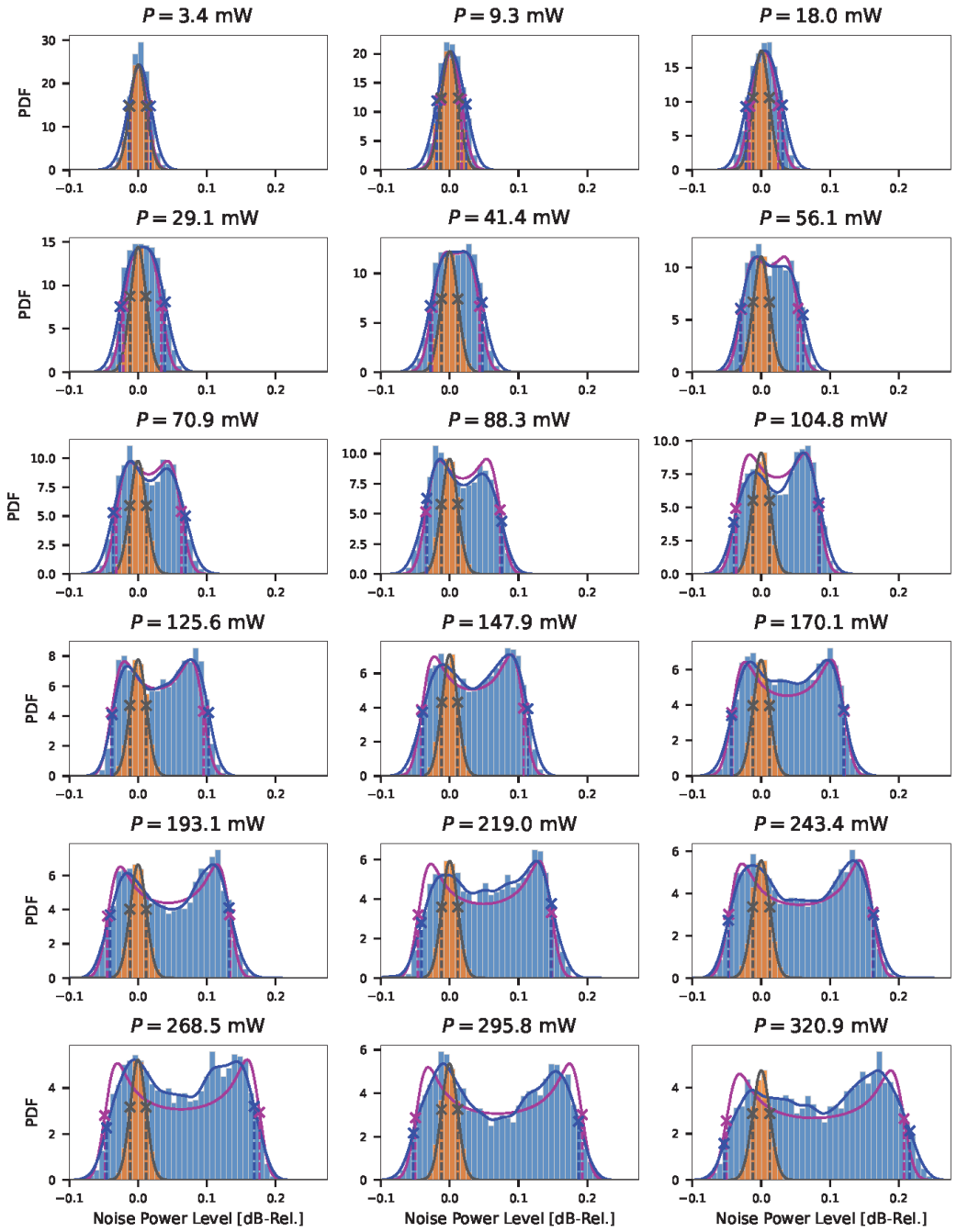

Figure C.4: Data analysis for the 32-channel source characterization in Fig. 6.5c: histograms of the sampled noise powers in Fig. C.3 for the squeezed vacuum (blue) and vacuum (orange) states. The KDE for the squeezed vacuum histogram is plotted in blue, the theoretical model of the PDF for the squeezed vacuum histogram is plotted in purple, and a Gaussian fit to the vacuum histogram is plotted in black. The locations of the maximum slopes for the squeezed state KDE, vacuum state Gaussian, and theoretical model are indicated with crosses and dashed lines, obtained from Fig. C.5.

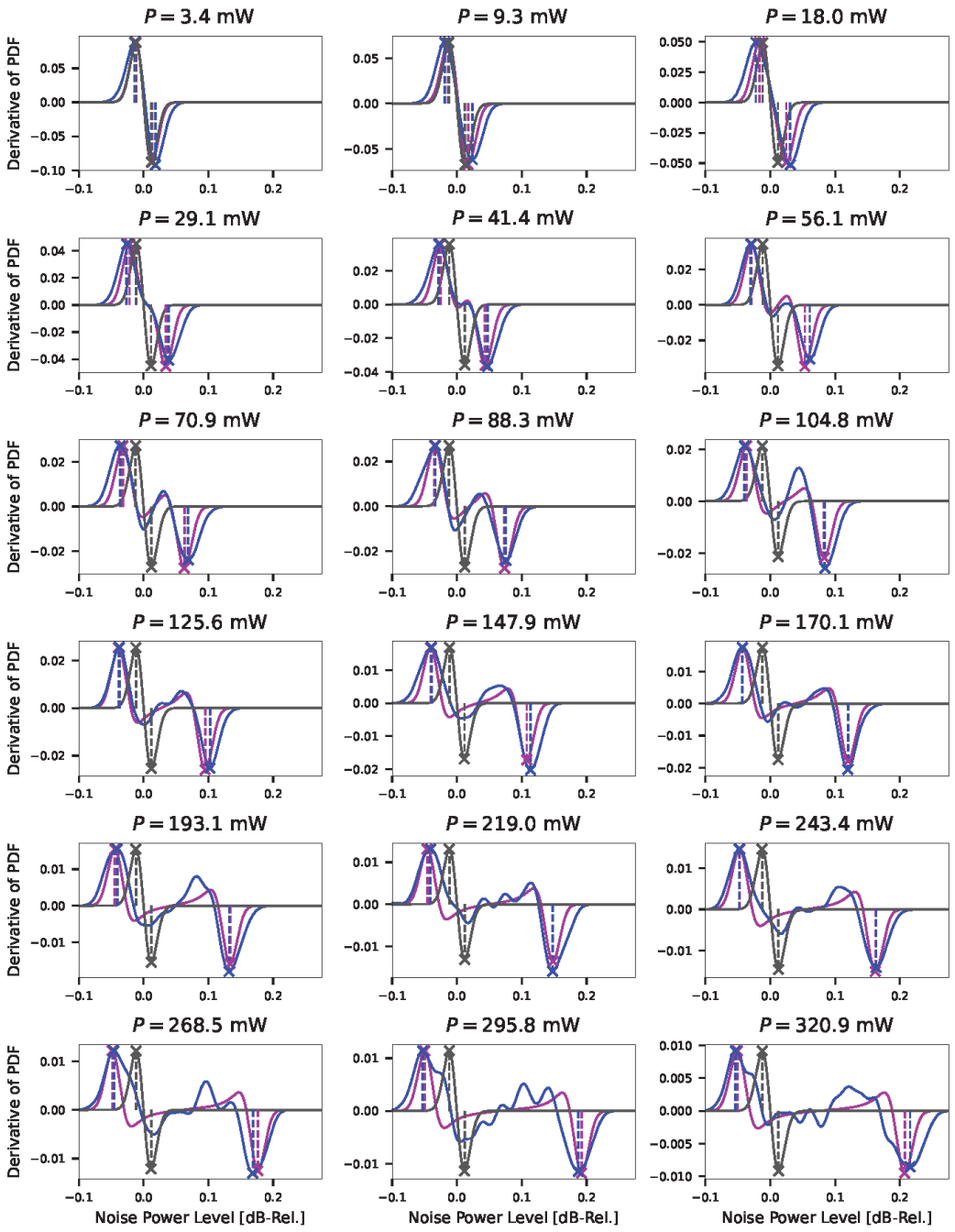

Figure C.5: Data analysis for the 32-channel source characterization in Fig. 6.5c: for each pump power in Fig. C.4, the derivative of the KDE for the squeezed vacuum histogram is plotted in blue, the derivative of the squeezed vacuum histogram is plotted in purple, and the derivative of the Gaussian fit to the vacuum histogram is plotted in black. The locations of the maxima and minima used to estimate the squeezing and antisqueezing levels are indicated with crosses and dashed lines.

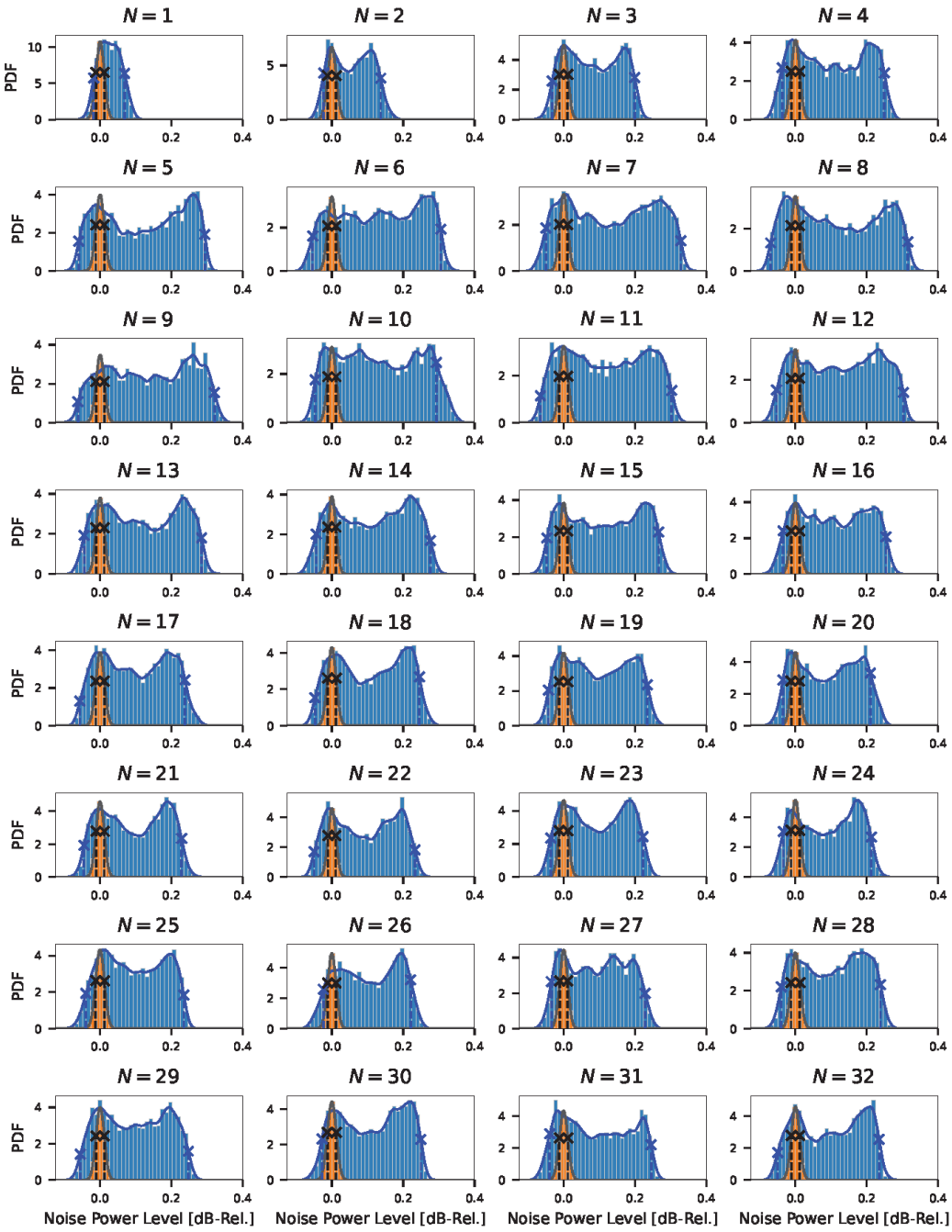

Figure C.6: Data analysis for beamforming in Fig. 6.5b: histograms of the sampled noise powers for the squeezed vacuum (blue) and vacuum (orange) states. The KDE for the squeezed vacuum histogram is plotted in blue and a Gaussian fit to the vacuum histogram is plotted in black. The locations of the peak slopes for the squeezed state KDE (blue) and vacuum state Gaussian (black) are indicated with crosses and dashed lines, which yield the squeezing/antisqueezing level estimates and the noise floor.

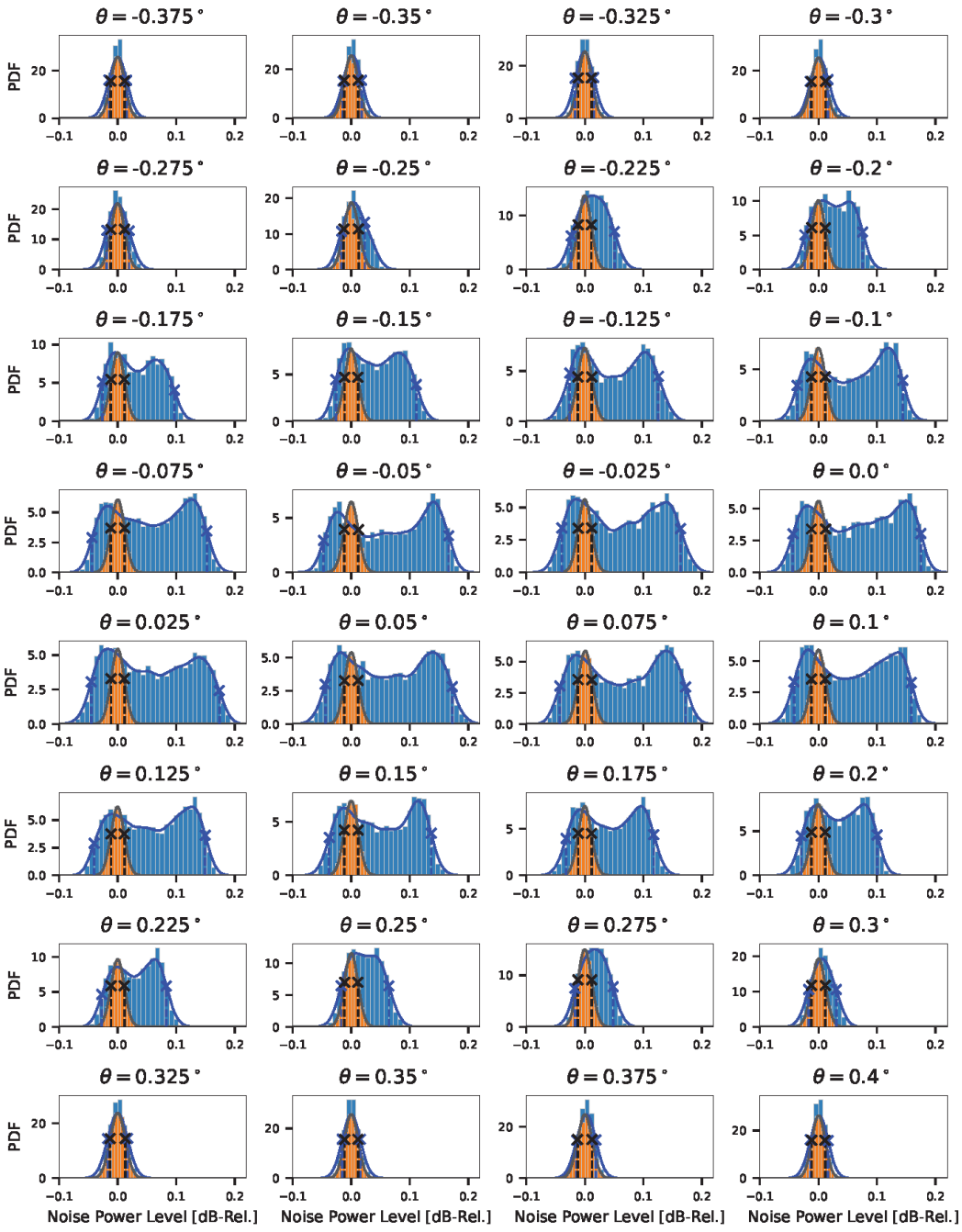

Figure C.7: Data analysis for the beamwidth characterization in Fig. 6.5e for 8 channels combined: histograms of the sampled noise powers for the squeezed vacuum (blue) and vacuum (orange) states are collected for various angles of incidence for a fixed beamforming angle (0°). The KDE for the squeezed vacuum histogram is plotted in blue and a Gaussian fit to the vacuum histogram is plotted in black. The locations of the peak slopes for the squeezed state KDE (blue) and vacuum state Gaussian (black) are indicated with crosses and dashed lines, which yield the squeezing/antisqueezing level estimates and the noise floor.

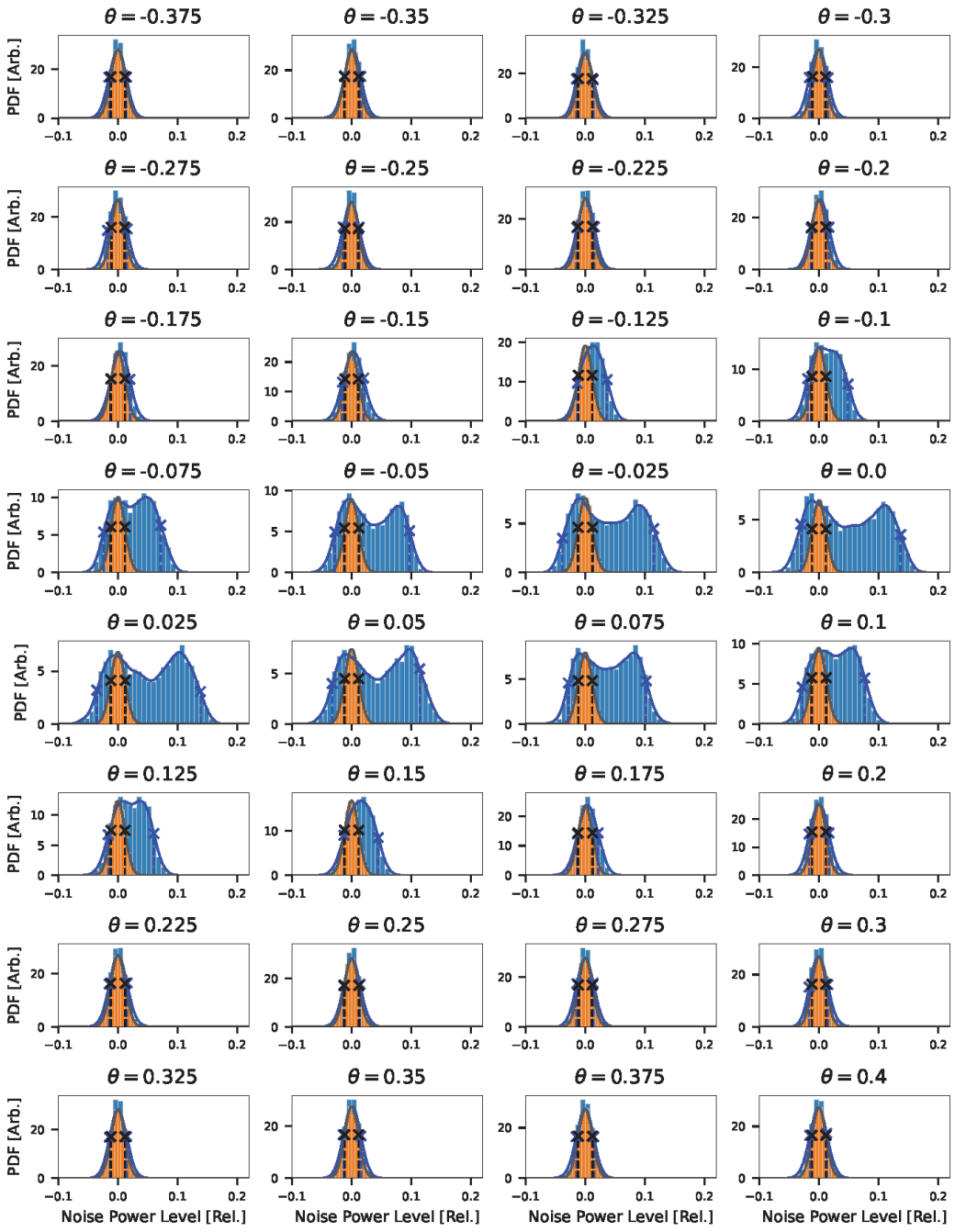

Figure C.8: Data analysis for the beamwidth characterization in Fig. 6.5e for 32 channels combined: histograms of the sampled noise powers for the squeezed vacuum (blue) and vacuum (orange) states are collected for various angles of incidence for a fixed beamforming angle (0°). The KDE for the squeezed vacuum histogram is plotted in blue and a Gaussian fit to the vacuum histogram is plotted in black. The locations of the peak slopes for the squeezed state KDE (blue) and vacuum state Gaussian (black) are indicated with crosses and dashed lines, which yield the squeezing/antisqueezing level estimates and the noise floor.

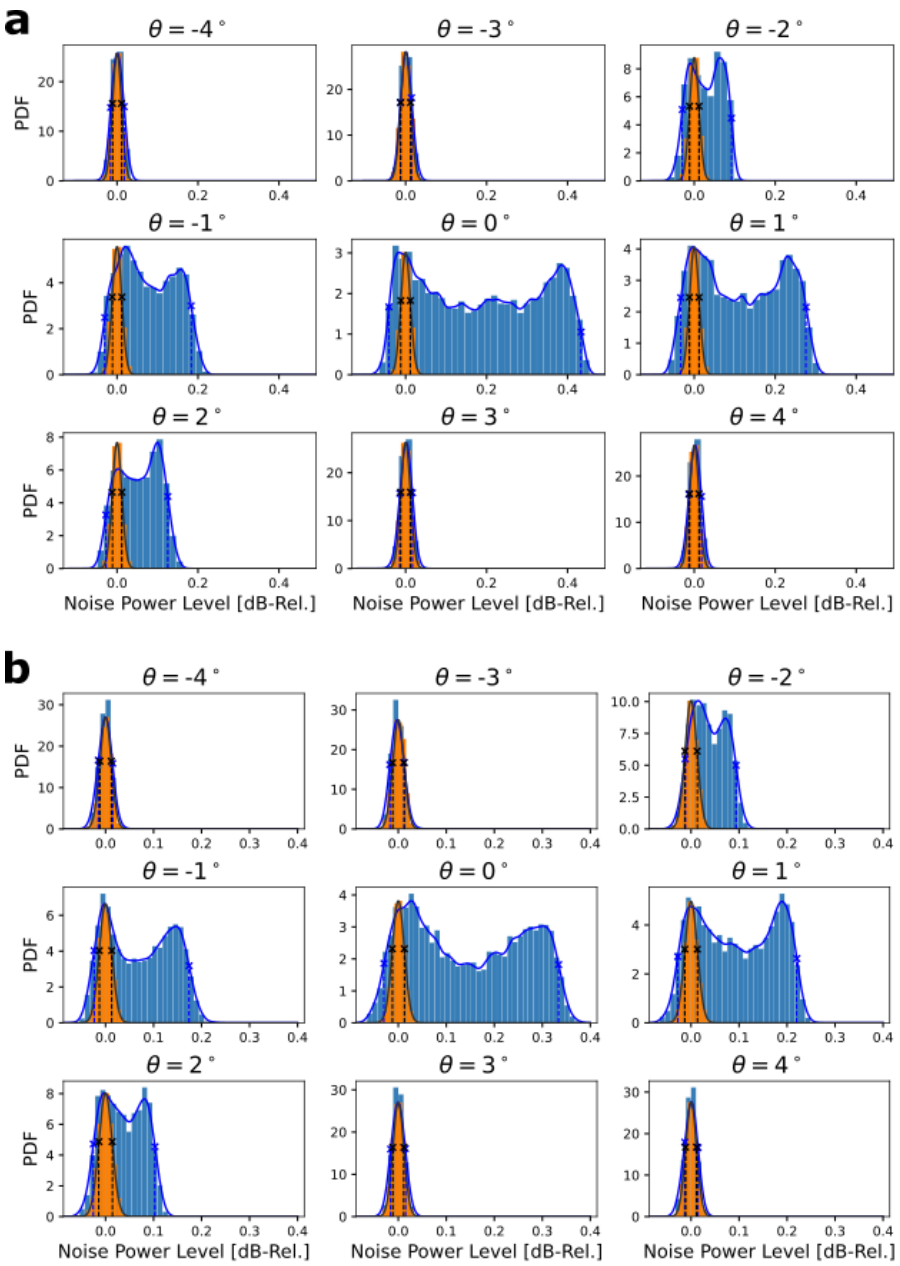

Figure C.9: Data analysis for the field-of-view characterization in Fig. 6.5f for a) 8 channels combined and b) 32 channels combined. Histograms of the sampled noise powers for the squeezed vacuum (blue) and vacuum (orange) states are collected for various angles of incidence, with beamforming performed at each angle. The KDE for the squeezed vacuum histogram is plotted in blue and a Gaussian fit to the vacuum histogram is plotted in black. The locations of the peak slopes for the squeezed state KDE (blue) and vacuum state Gaussian (black) are indicated with crosses and dashed lines, which yield the squeezing/antisqueezing level estimates and the noise floor.

C.2 Squeezed light source characterization

The squeezed light sources are characterized with a modified version of the transmitter setup from Chapter 6 as shown in Fig. C.10a. Continuous wave light from a fiber-coupled 1550 nm laser (OEWaves) is split into a signal path and a local oscillator (LO) path. The light in the signal path is sent to an erbium-doped fiber amplifier (PriTel EDFA) with a tunable gain. The amplified light is upconverted to 775 nm by second harmonic generation (SHG) with a periodically poled lithium niobate (PPLN) waveguide. The upconverted light is sent to another PPLN waveguide for Type 0 spontaneous parametric downconversion (SPDC) to generate squeezed light centered at 1550 nm. The squeezed light is sent to an isolator (Thorlabs), which rejects back-reflected light and serves as a filter for any residual 775 nm pump light. After the isolator, an optical switch is used to switch between the vacuum and squeezed vacuum state measurements. The squeezed light is sent to a polarization-maintaining 50:50 beamsplitter (BS) for interference with the LO.

In the LO path, the 1550 nm laser light is sent to an electro-optic phase modulator (EOSpace) to apply a phase ramp to the LO. The phase ramp is generated by sending a modulated signal from a function generator to the RF input of the modulator. After the modulator, a polarizing beamsplitter (PBS) removes light polarized along the fast axis to ensure interference in a single polarization mode at the beamsplitter. The outputs of the beamsplitter are sent to a fiber-coupled balanced homodyne detector (BHD). The BHD (Thorlabs PDB425C) has a 75 MHz bandwidth, 35 dB CMRR, and 1 A/W responsivity. The RF output of the BHD is sent to an RF spectrum analyzer (Keysight N9030b) operated in zero-span mode to measure the noise power levels in real time.

A total of four PPLN waveguides were used for SPDC in the experiments of the main text. The four experimental configurations are summarized in Table C.1. For each configuration, a pump power sweep was performed to characterize the SPDC waveguide and the effective efficiency of the setup [1]. For SPDC, the waveguide-coupled 775 nm pump power (P) can be related to the squeezing parameter (r) by $r \approx \mu\sqrt{P}$ [2], where μ is the SPDC efficiency [3]. The amount of squeezing can be characterized experimentally by comparing the variance of the quadratures measured with a squeezed state input to that measured with a vacuum state input in homodyne detection,

$$\frac{\langle \Delta\hat{Q}(\phi)^2 \rangle_{\text{sq}}}{\langle \Delta\hat{Q}(\phi)^2 \rangle_{\text{vac}}} = \eta(e^{-2r}\cos^2\phi + e^{2r}\sin^2\phi) + 1 - \eta. \tag{C.1}$$

From Eq. C.1, the squeezing (ΔQ_-^2) and antisqueezing (ΔQ_+^2) levels relative to the shot noise level in terms of the pump power are,

$$\Delta Q_\pm^2 = \eta \exp\left(\pm 2\mu\sqrt{P}\right) + 1 - \eta, \tag{C.2}$$

where η is the effective efficiency, including the effects of source loss, fiber-optic loss, detector loss, and shot noise clearance. For each pump power, the noise levels for the squeezing vacuum and vacuum states were measured over multiple LO phases. The pump power was varied by tuning the gain of the EDFA. To characterize the SPDC waveguide in configuration 1, an EDFA with up to 27 dBm output power was used, and to characterize the SPDC waveguides in configurations 2-4, an EDFA with up to 37 dBm output power was used. A phase ramp was applied to the LO to ensure that noise power levels were accumulated over multiple periods. The squeezing and antisqueezing levels for all configurations were estimated from the noise power distribution using the procedure described in Appendix B.

The characterizations for the four sources are shown in Fig. C.10b-e. The squeezing and antisqueezing estimates are plotted as a function of the waveguide-coupled power, which is calculated from,

$$P = \eta_{in} P_{\mathrm{SHG}}, \tag{C.3}$$

where η_{in} is the 775 nm input coupling efficiency and P_{SHG} is the power measured at the output of the SHG. The red curves are the theoretical model for the squeezing and antisqueezing levels from Eq. C.2. The best-fit parameters η and μ are obtained from a simultaneous least squares fit to the squeezing and antisqueezing levels. The errorbars are calculated from the Jacobian, and the residuals are evaluated at the optimal parameters. The key specifications for the four SPDC waveguides are summarized in Table C.2. The fitted effective efficiencies η of Fig. C.10b-e include the waveguide output coupling efficiencies η_{out} reported in Table C.2 as well as all other system losses (see Sec. C.4).

C.3 Measurement characterization

Squeezed light imaging

Data acquisition and analysis To image the squeezed light incident on the chip, we collect quadrature statistics of each antenna field mode over various phases by applying a 2π phase ramp on the LO at 0.5 Hz. The RF outputs from each QRX

Config.	SHG waveguide	SPDC waveguide	Experiments
1	Covesion H-spec.	HCP SC18068	Fig. 6.4c
2	HCP SC23399	Covesion H-spec.	Fig. 6.5b,c
3	HCP SC23399	HCP SC19075	Fig. 6.5f
4	HCP SC23399	Covesion M-spec.	Fig. 6.5e

Table C.1: Waveguide configurations used in experiments of Chapter 6. Configuration 1 was used for squeezed light imaging (Fig. 6.4c). Configuration 2 was used for beamforming channel sweep (Fig. 6.5b) and 32-channel pump power sweep (Fig. 6.5c). Configuration 3 was used for the field-of-view data (Fig. 6.5f). Configuration 4 was used for the beamwidth data (Fig. 6.5e).

SPDC waveguide	η_{in}	η_{out}	L (cm)	μ [mW$^{-1/2}$]
HCP SC18068	0.4	0.4	3	0.119
Covesion H-spec.	0.7	0.8	4	0.038
HCP SC19075	0.4	0.4	3	0.070
Covesion M-spec.	0.7	0.8	4	0.031

Table C.2: PPLN waveguides used as sources of squeezed light. η_{in} is the 775 nm input coupling efficiency, η_{out} is the 1550 nm output coupling efficiency, and μ is the SPDC efficiency obtained from a least-squares fit to the pump power sweep data in Fig. C.10.

are digitized and stored at a sampling rate of 20 MSa/s over 4 seconds. A digital bandpass filter with a 2 MHz bandwidth is applied to the digital data. The data is then passed through a moving mean and variance filter with a bin size of 260,000 and is downsampled by a factor of 16,000 to obtain the sample means and variances.

Squeezing parameter estimation The squeezing parameter was estimated with the source characterization setup of Fig. C.10 in Configuration 1. Five-second traces of the squeezed vacuum and vacuum noise power levels immediately before transmission to the chip are shown in Fig. C.11a. The corresponding histograms, kernel density estimates (KDEs), and derivatives of the KDEs are in C.11b-c. The estimates for the squeezed state are indicated with the blue crosses. From the squeezing estimate of -0.695 ∓ 0.029 dB and antisqueezing estimate of 9.158 ± 0.029 dB, we obtain $r = 1.945^{-0.006}_{+0.015}$ and $\eta = 0.151^{+0.003}_{-0.006}$.

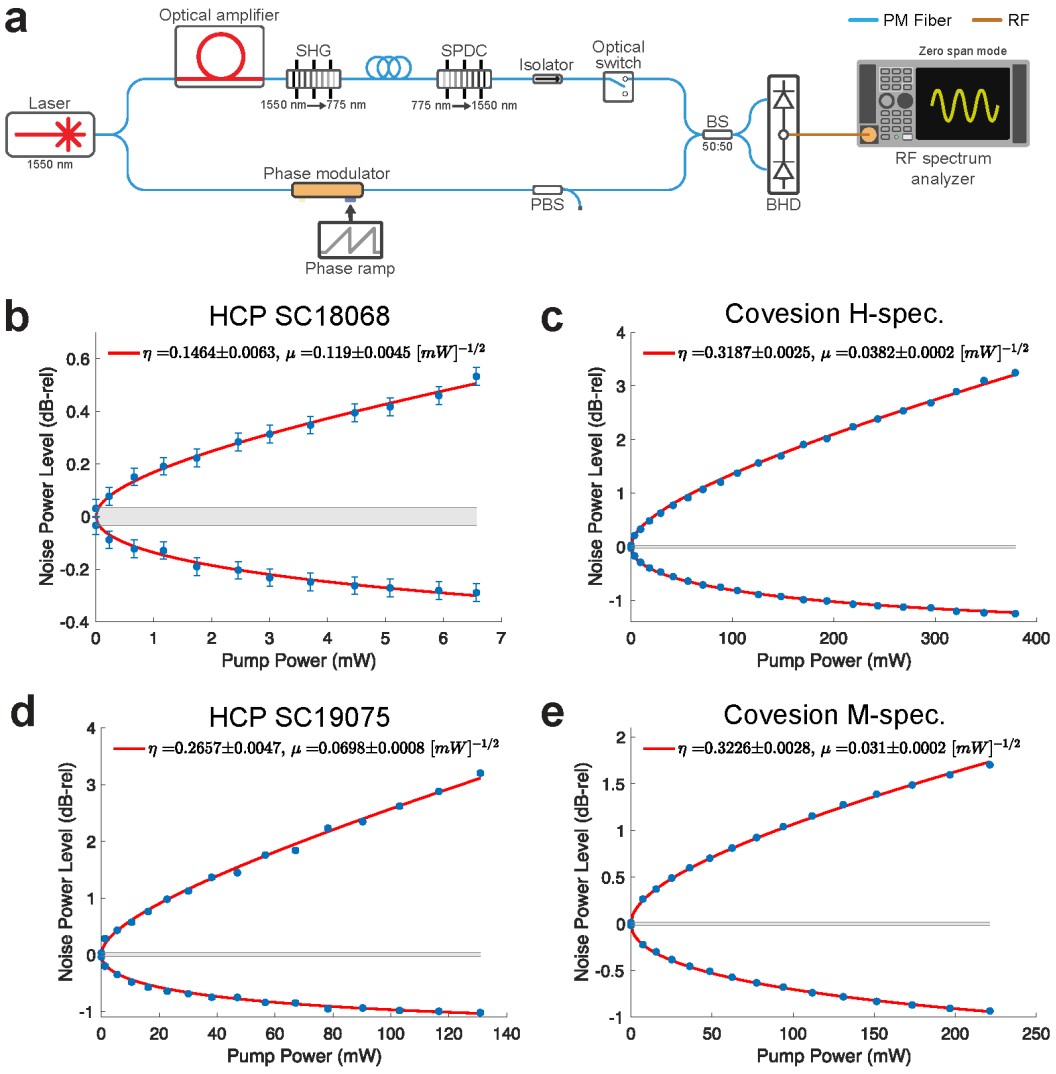

Figure C.10: Squeezed light source characterization. a) Experimental setup for source characterization. b) Configuration 1. Each noise power trace was measured over 10s with a sampling rate of 10 kHz, center frequency of 6 MHz, 1 MHz RBW, and 20 Hz VBW. c) Configuration 2. Each noise power trace was measured over 10s at 1 Hz phase modulation with a sampling rate of 5 kHz, 40 MHz CF, 8 MHz RBW, and 100 Hz VBW. d) Configuration 3. Each noise power trace was measured over 5s at 1 Hz phase modulation with a sampling rate of 20 kHz, 4 MHz CF, 20 MHz RBW, and 10 Hz VBW. e) Configuration 4. Each noise power trace was measured over 10s at 1 Hz phase modulation with a sampling rate of 10 kHz, 20 MHz CF, 8 MHz RBW, and 30 Hz VBW.

These numbers are within the error bars of the prediction from the source characterization of the SPDC waveguide (HCP SC18068). From the least-squares fit to

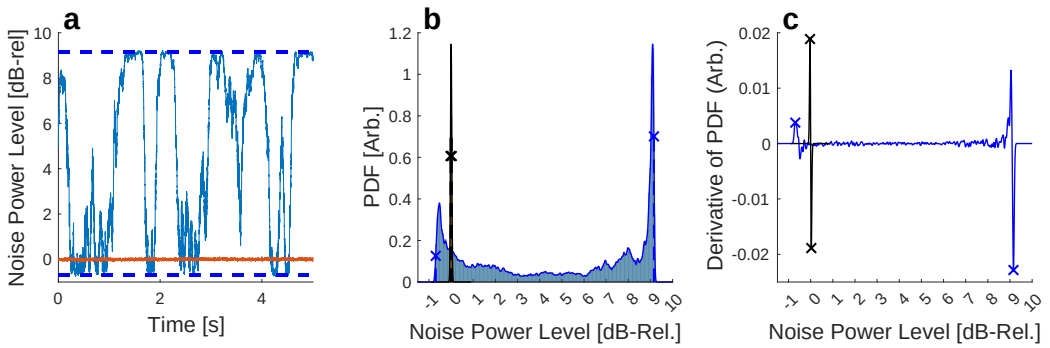

Figure C.11: Characterization of squeezing for squeezed light imaging. a) A five-second snippet of noise power levels for squeezed vacuum (blue) and vacuum (orange) measured at the source immediately before imaging. The noise powers were measured with a sampling rate of 20 kHz, center frequency of 6 MHz, 8 MHz RBW, and 100 Hz VBW. b) Histograms for the squeezed vacuum (light blue) and vacuum (orange) for the noise powers accumulated in a). The kernel density estimates (KDEs) for the squeezed vacuum (blue) and vacuum (black) histograms are plotted as solid lines. c) Derivative of KDEs for squeezed vacuum (blue) and vacuum (black).

the data in Fig. C.10a, $\eta = 0.146$ and $\mu = 0.119$ $[\mathrm{mW}]^{-1/2}$. For the waveguide-coupled pump power of $P = 315.6 \pm 47.3$ mW, the estimated squeezing parameter is $r = 2.114 \pm 0.159$.

Phase estimation The phases for the Wigner functions of the 32 antenna modes are found by performing a sinusoidal fit to a portion of the data with an approximately uniform phase ramp. The data and fits are shown in Fig. C.12.

Channel effective efficiency estimation The channel effective efficiencies are calculated from

$$\eta = \frac{(A-1)\exp(2r)}{(\exp(2r)-1)(A+\exp(2r))}, \tag{C.4}$$

where $A = \Delta Q_+^2/\Delta Q_-^2$ is the ratio of the antisqueezing (ΔQ_+^2) to squeezing (ΔQ_-^2) levels and $r = 1.945$. The ratio of antisqueezing to squeezing is obtained from the amplitudes of the sinusoidal fits in Fig. C.12. The channel effective efficiencies are plotted in Fig. C.13. For the Wigner functions, the geometric efficiency ($\eta_j^{(g)}$) for channel j is calculated as $\eta_j^{(g)} = \eta_j/\sum_j \eta_j$, where $\sum_j \eta_j = 0.017$. A Gaussian fit to the data yields a standard deviation of $\sigma = 48.8 \pm 2.5$ μm. This corresponds to

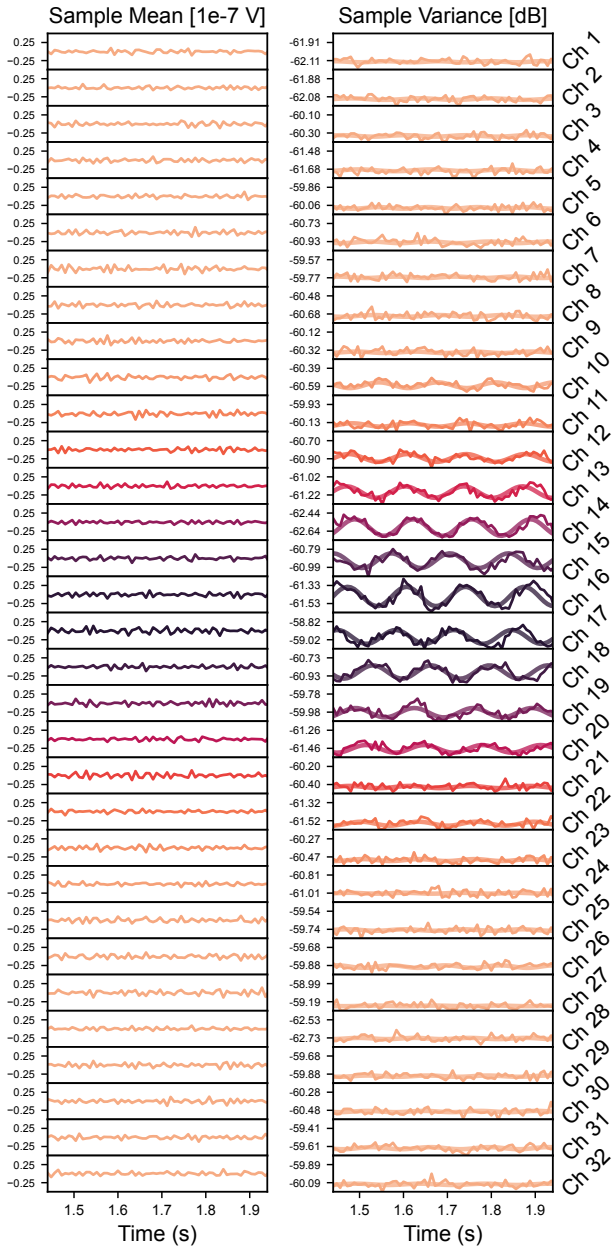

Figure C.12: Quadrature sample means and variances over time for all 32 channels. The sample means are approximately zero, while sinusoidal variations are observed in the sample variances. The fits to the variances are plotted as transparent solid lines.

a Gaussian beam diameter of $4\sigma = 195.2 \pm 10$ μm, consistent with the collimator beam diameter of 200 μm.

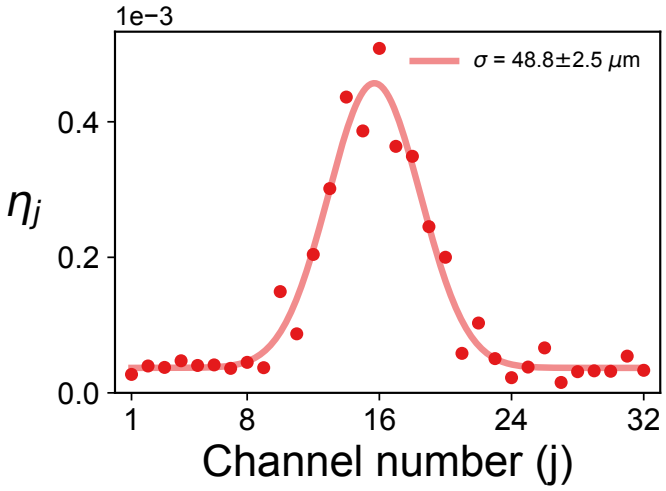

Figure C.13: Channel effective efficiencies versus channel number. The solid line is a Gaussian fit to the data.

Classical imaging

Replacing the transmitted squeezed vacuum state with a coherent state allows us to operate the chip in a classical mode, compatible with previously demonstrated classical imaging schemes [4]. This enables hybrid quantum-classical operation of the chip and comparisons of squeezed light measurements with classical measurements. In the case of imaging, we send a 1550 nm coherent state to the aperture through the collimator and apply 5 MHz phase modulation to the LO. The classical SNR is the same as effective efficiency (η), characterizing the decoherence of the quantum state in the receiver chain. Therefore, we approximate the classical SNR of this 5 MHz downconverted signal as a classical comparison to the squeezed light data. 32-channel RF outputs are digitized by a 32-channel digitizer with a sampling rate of 100 MSa/s. 10 ms of data are collected for each channel simultaneously using the same electronic readout as the squeezed light imaging measurement. By recording the outputs with and without sending light to the aperture, signal, and noise traces are collected for all 32 channels, as seen in Fig. C.14a. The raw traces are filtered with a digital bandpass filter with a center frequency of 5 MHz and a bandwidth of 100 kHz. We take the Hilbert transform of the filtered signal data to extract the analytical signal and the amplitude for each signal trace is determined, as seen in Fig. C.14b. Similarly, variances of the filtered noise data are measured and plotted

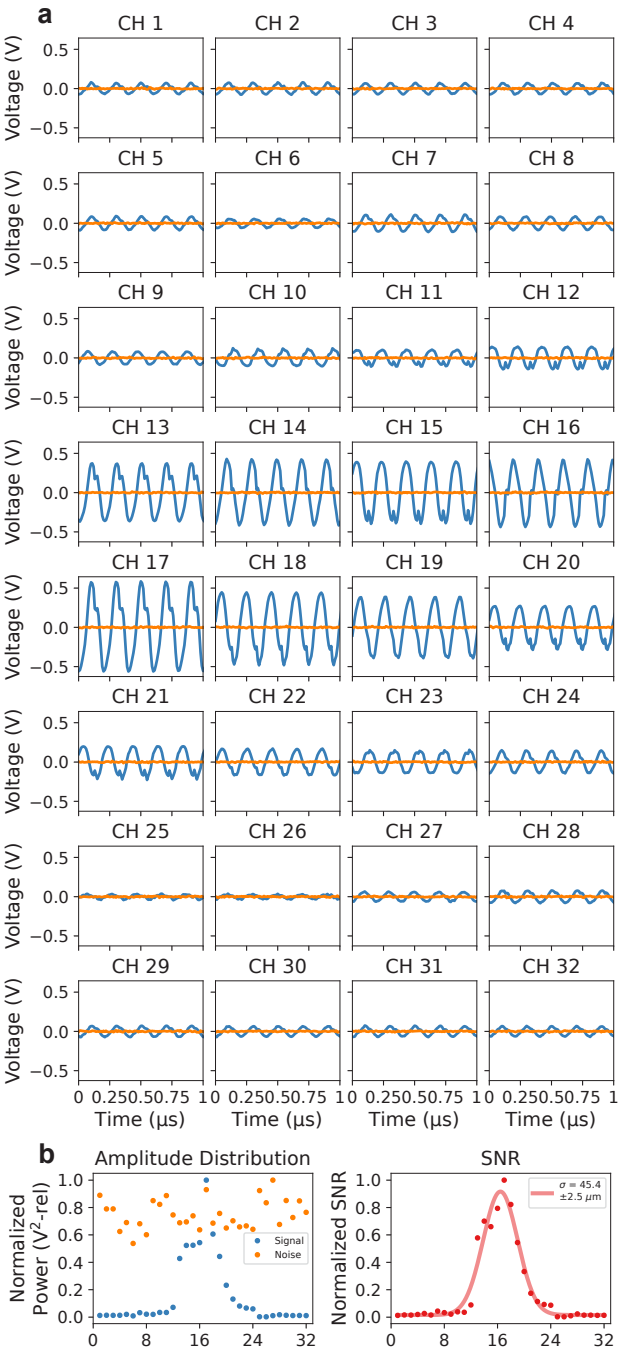

Figure C.14: Classical imaging characterization with coherent light. a) An example of signal (blue) and noise (orange) time-domain traces recorded for 32 channels. b) Extracted signal and noise powers across 32 channels in the frequency range of the downconverted tone and the corresponding SNR.

in Fig. C.14b. The ratio between these amplitudes gives the SNR, which is plotted in Fig. C.14c. A Gaussian fit is applied to the SNR data, which extracts a standard

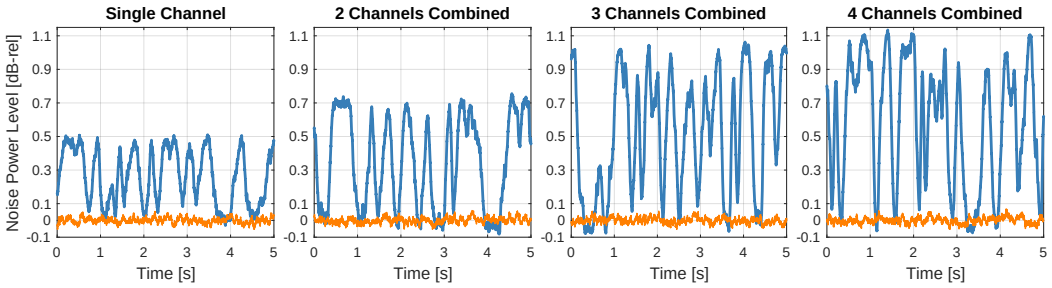

Figure C.15: Beamforming on-chip with the HCP SC18068 waveguide used for SPDC.

deviation of $\sigma = 45.4 \pm 2.5$ μm.

Beamforming and pump power sweep

The beamforming (Fig. 6.5b) and 32-channel source characterization (Fig. 6.5c) data of the main text were performed with the source in Configuration 2, using the Covesion H-spec waveguide for SPDC. The beamforming sweep was performed at a waveguide-coupled pump power of $P = 383.3 \pm 19.2$ mW. From the Covesion H-spec characterization in Sec. C.2, this corresponds to a squeezing parameter of $r = 0.748 \pm 0.019$.

Before performing the full 32-channel sweep, we first performed beamforming up to four channels using the HCP SC18068 waveguide for SPDC. A pump power of 226.8 ± 22.7 mW was coupled onto the waveguide, corresponding to a squeezing parameter of $r = 1.792 \pm 0.090$. The data are shown in Fig. C.15.

Classical channel sweep

The classical SNR data to extract the estimated efficiencies for the channel sweep (Fig. 6.5b) of the main text is done by using the same electronic readout with the ESA. We send a 1550 nm coherent state to the aperture through the collimator and apply 5 MHz phase modulation to the LO. We measure the downconverted 5 MHz signal in the ESA for each channel combination ($[1, 2, 4, \cdots, 30, 32]$ channels) as seen in Fig. C.16a (left). The video bandwidth for the signal measurements is 1 Hz, and the resolution bandwidth is 100 Hz. We also measure the noise powers for each channel combination using the ESA in zero-span mode at a center frequency of 5 MHz, with a resolution bandwidth of 2 MHz and a video bandwidth of 5 Hz as seen in Fig. C.16a (right). After collecting these traces, we measure the signal and noise amplitudes as seen in Fig. C.16b (left). For the signal amplitudes, we measure the

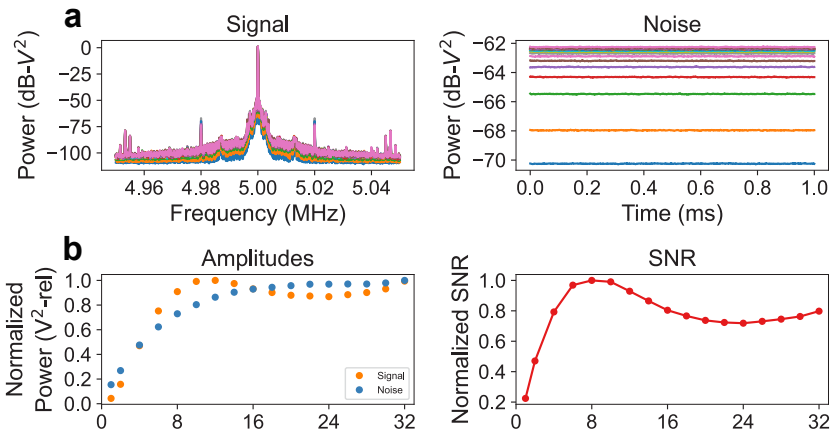

Figure C.16: Classical channel sweep characterization with coherent light. a) Signal (left) and noise (right) data recorded in the frequency domain for $[1, 2, 4, \cdots, 30, 32]$ channel combinations for the measurement in Fig. 6.5b. b) Extracted signal and noise powers (left) in the frequency range of the downconverted tone and the corresponding SNR (right).

total power in the frequency range between 4.95 MHz to 5.05 MHz in the collected data. For the noise amplitudes, we measure the mean power in the noise floor. We then extract the normalized SNR by taking the ratio of these amplitudes and normalizing the values as seen in Fig. C.16b (right). The resulting values are used to plot the expected squeezing and antisqueezing using Eq. C.1 with the squeezing parameter extracted from source characterization. For the proportionality constant, we apply a least-squares fit with η as the floating parameter with the squeezing parameter bounded as $r = 0.748 \pm 0.019$ to fit the resulting plot to the data, yielding a proportionality constant of $\eta_c = 0.021$.

Beamwidth

The beamwidth measurement (Fig. 6.5e) of the main text was performed with the source in Configuration 4, using the Covesion M-spec waveguide for SPDC. The beamwidth data were taken at a waveguide-coupled pump power of $P = 383.6 \pm 19.7$ mW. From the Covesion M-spec characterization in Sec. C.2, this corresponds to a squeezing parameter of $r = 0.607 \pm 0.015$.

Classical beamwidth

The classical SNR data to extract the estimated efficiencies for the beamwidth measurements (Fig. 6.5e) of the main text is done by using the same electronic

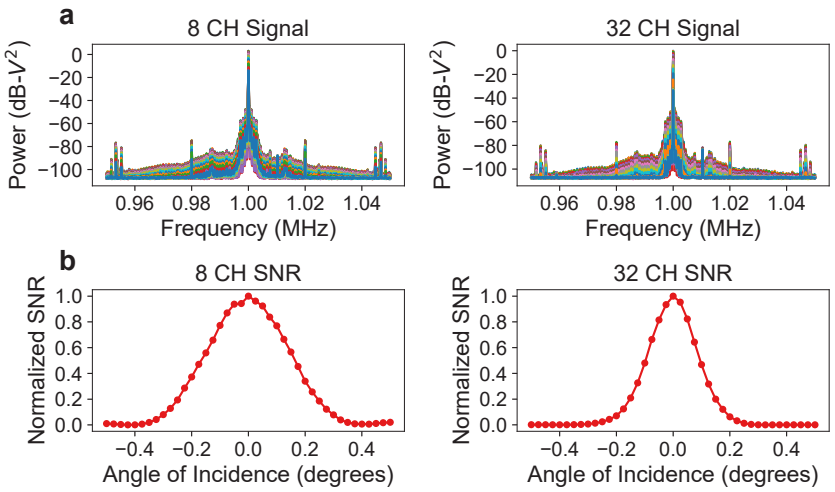

Figure C.17: Classical beamwidth characterization with coherent light. a) Signal data recorded in the frequency domain for different angles of incidence for 8 (left) and 32 (right) channels combined for the measurement in Fig. 6.5e. b) Extracted signal powers corresponding to normalized SNR in the frequency range of the downconverted tone for 8 (left) and 32 (right) channels combined.

readout with the ESA. We send a 1550 nm coherent state to the aperture through the collimator and apply 1 MHz phase modulation to the LO. We measure the downconverted 1 MHz signal in the ESA for each incidence angle for both 8 channels and 32 channels combined, as seen in Fig. C.17a. The video bandwidth for the signal measurements is 1 Hz, and the resolution bandwidth is 100 Hz. Since the electronic configuration for these measurements stays the same, the noise floor doesn't change, making signal directly proportional to SNR. Using the measured spectra in Fig. C.17a, we measure the total power in the frequency range between 0.95 MHz to 1.05 MHz to acquire the signal amplitudes proportional to SNR for both 8 channels and 32 channels combined, as seen in Fig. C.17b. The resulting values are used to plot the expected squeezing and antisqueezing using Eq. C.1 with the squeezing parameter extracted from source characterization. For the proportionality constant, we apply a least-squares fit with η as the floating parameter and the squeezing parameter bounded as $r = 0.607 \pm 0.0152$ to fit the resulting plot to the data, yielding an optimal squeezing parameter of $r = 0.611$ and proportionality constants of $\eta_c^{(8)} = 0.0191$ and $\eta_c^{(32)} = 0.0141$ for 8 and 32 channels combined, respectively.

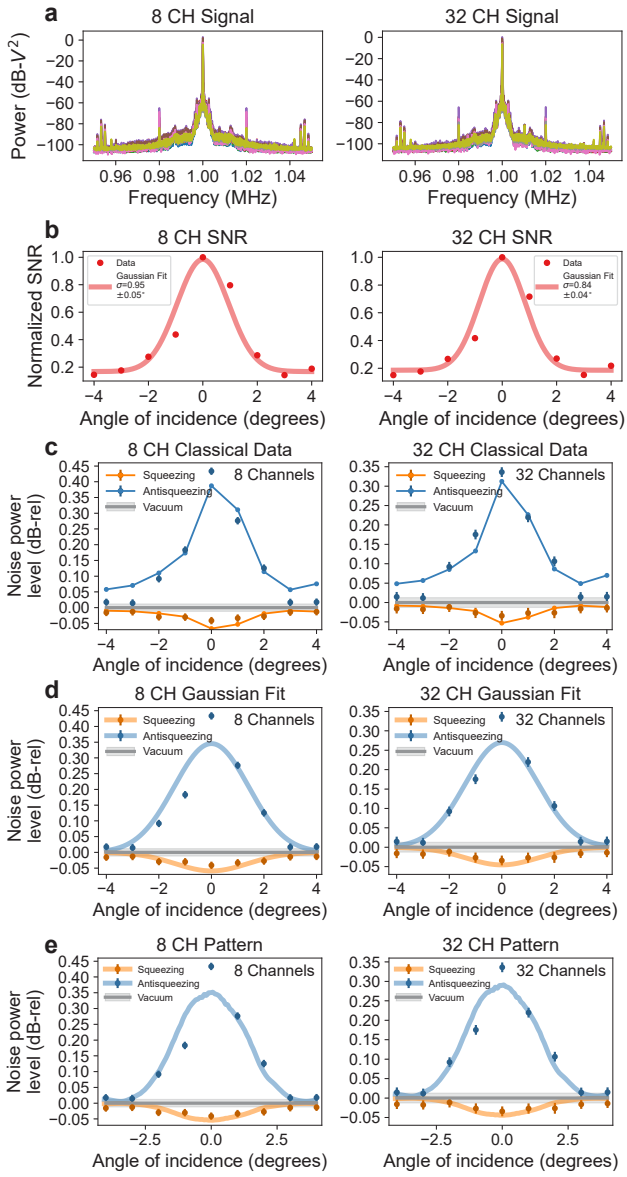

Figure C.18: Classical field-of-view characterization with coherent light. a) Signal data recorded in the frequency domain for different angles of incidence for 8 (left) and 32 (right) channels combined for the measurement in Fig. 6.5f. b) Extracted signal powers corresponding to normalized SNR in the frequency range of the downconverted tone for 8 (left) and 32 (right) channels combined. A Gaussian fit is applied to the data, yielding σ =0.95±0.05° and σ =0.84±0.04° for 8 and 32 channels combined, respectively. c) Comparison of the classical data to the squeezed light data for 8 (left) and 32 (right) channels combined. d) Comparison of the Gaussian fit of the classical data to the squeezed light data for 8 (left) and 32 (right) channels combined. e) Comparison of single antenna radiation pattern to the squeezed light data for 8 (left) and 32 (right) channels combined, repeated from Fig. 6.5f.

Field of view

The field-of-view (FoV) experiment (Fig. 6.5f) of the main text was performed with the source in Configuration 3, using the HCP SC19075 waveguide for SPDC. The FoV data were taken at a waveguide-coupled pump power of $P = 153.4 \pm 15.3$ mW. From the HCP SC19075 characterization in Sec. C.2, this corresponds to a squeezing parameter of $r = 0.865 \pm 0.043$.

Classical field of view

Multiple approaches were taken to acquire the classical comparison for the FoV measurement (Fig. 6.5f) of the main text. The single antenna radiation pattern is an accurate classical estimate of the full array pattern since the aperture is fully filled, and the electronic configuration stays the same for each angle of incidence. Therefore, the classical comparison in Fig. 6.5f uses the measured far-field single antenna radiation pattern. We normalize this pattern and set it to be proportional to SNR. The resulting values are used to plot the expected squeezing and antisqueezing using Eq. C.1 with the squeezing parameter extracted from source characterization, as shown in Fig. 6.5f and also in Fig. C.18e. For the proportionality constant, we apply a least-squares fit with η as the floating parameter and with the squeezing parameter bounded as $r = 0.865 \pm 0.043$ to fit the resulting plot to the data, yielding an optimal squeezing parameter of $r = 0.908$ and proportionality constants of $\eta_c^{(8)} = 0.0167$ and $\eta_c^{(32)} = 0.0152$ for 8 and 32 channels combined, respectively.

A beamformed classical measurement is also taken for each of the 9 angles in the FoV measurement. For classical FoV measurement, we send a 1550 nm coherent state to the aperture through the collimator and apply 1 MHz phase modulation to the LO. We measure the downconverted 1 MHz signal in the ESA for each angle of incidence for both 8 channels and 32 channels combined, as seen in Fig. C.18a. The video bandwidth for the signal measurements is 1 Hz, and the resolution bandwidth is 100 Hz. Since the electronic configuration for these measurements stays the same, the noise floor doesn't change, making signal directly proportional to SNR. Using the measured spectra in Fig. C.18a, we measure the total power in the frequency range between 0.95 MHz to 1.05 MHz to acquire the signal amplitudes proportional to SNR for both 8 channels and 32 channels combined as seen in Fig. C.18b. The resulting values are used to plot the expected squeezing and antisqueezing using Eq. C.1 with the squeezing parameter extracted from source characterization. For the proportionality constant, we apply a least-squares fit with η as the floating

parameter and with the squeezing parameter bounded as $r = 0.865 \pm 0.043$ to fit the resulting plot to the data, yielding an optimal squeezing parameter of $r = 0.908$ and a proportionality constant of $\eta_c^{(8)} = 0.0181$ and $\eta_c^{(32)} = 0.0145$ for 8 and 32 channels combined, respectively. The comparison of the classical data to the squeezed light data in Fig. 6.5f of main text is shown in Fig. C.18c. We also fit the classical data to a Gaussian function, yielding a standard deviation of 0.95±0.05 degrees and 0.84±0.04 degrees for 8 and 32 channels combined, respectively. The comparison of the Gaussian fit to the squeezed light data is shown in Fig. C.18d.

A linear interpolation is used to extract the classical FoV to directly compare with the FoV extracted from squeezed light data in the main text. With linear interpolation on the classical data, we extract an FoV of 2.5 degrees and 2.3 degrees for 8 and 32 channels combined, respectively. These classical estimates match well with the squeezed light FoV of 2.3 degrees and 2.7 degrees for 8 and 32 channels combined, respectively, in the main text. The discrepancy between classical and squeezed light data is due to the measurements being taken sequentially. Future schemes in which classical and non-classical light are multiplexed in the same link [5] would minimize this discrepancy.

C.4 Loss budget

We characterize the measurement setup losses for each experiment (see Supplementary Information of Ref. [6]) and report them here. A summary of the system losses for each measurement setup is in Table C.3.

Experiment	Source loss (dB)	Free-space loss (dB)	On-chip loss (dB)	RF loss (dB)	Total loss (dB)
Imaging	8.17	1.14	5.72	0.137	15.2
Channel sweep	6.97	2.18	5.72	0.660	15.5
Power sweep	6.97	4.85	5.72	2.16	19.7
BW (8CH)	6.97	2.18	5.72	0.306	15.2
BW (32CH)	6.97	4.85	5.72	1.43	19.0
FoV (8CH)	6.90	2.18	5.72	1.21	16.1
FoV (32CH)	6.90	4.85	5.72	2.13	19.6

Table C.3: Measurement system losses for each experiment. The table breaks down loss contributions from the source, free-space link, on-chip photonic circuit, and RF readout electronics.

References

[1] Henning Vahlbruch, Moritz Mehmet, Karsten Danzmann, and Roman Schnabel. "Detection of 15 dB squeezed states of light and their application for the absolute calibration of photoelectric quantum efficiency." In: Physical Review Letters 117.11 (2016), p. 110801.

[2] T. Hirano, K. Kotani, T. Ishibashi, S. Okude, and T. Kuwamoto. "3 dB squeezing by single-pass parametric amplification in a periodically poled KTiOPO4 crystal." In: Opt. Lett. 30.13 (July 2005), pp. 1722–1724.

[3] Florian Kaiser, Bruno Fedrici, Alessandro Zavatta, Virginia d'Auria, and Sébastien Tanzilli. "A fully guided-wave squeezing experiment for fiber quantum networks." In: Optica 3.4 (2016), pp. 362–365.

[4] Christopher Rogers, Alexander Y. Piggott, David J. Thomson, et al. "A universal 3D imaging sensor on a silicon photonics platform." In: Nature 590.7845 (Feb. 2021), pp. 256–261.

[5] R Valivarthi, P Umesh, C John, K A Owen, V B Verma, S W Nam, D Oblak, Q Zhou, and W Tittel. "Measurement-device-independent quantum key distribution coexisting with classical communication." In: Quantum Science and Technology 4.4 (July 2019), p. 045002.

[6] Volkan Gurses, Samantha I. Davis, Raju Valivarthi, Neil Sinclair, Maria Spiropulu, and Ali Hajimiri. "An on-chip phased array for non-classical light." In: Nature Communications 16.1 (2025), p. 6849.